

# Form of Deprotection in Chemically Amplified Resists

Ronald L. Jones<sup>a</sup>, Tengjiao Hu<sup>a</sup>, Vivek M. Prabhu<sup>a</sup>, Christopher L. Soles<sup>a</sup>, Eric K. Lin<sup>a</sup>, Wen-li Wu<sup>a</sup>, Dario L. Goldfarb<sup>b</sup>, Marie Angelopoulos<sup>b</sup>

<sup>a</sup>Polymers Division, National Institute of Standards and Technology, Gaithersburg, MD 20899

<sup>b</sup>IBM T.J. Watson Research Center, Yorktown Heights, NY 10598

**Abstract.** The push to mass production of patterns with sub-100 nm dimensions will require nanometer level control of feature size, including line edge roughness (LER). Control of LER and sidewall roughness within the length scale of individual molecules requires a fundamental understanding of LER formation. For chemically amplified resists, image quality is controlled in part by the diffusion and reaction of small molecule photogenerated acids within the resist. Using Small Angle Neutron Scattering (SANS) we provide a direct measurement of the form of the deprotection path created by individual acid molecules common to chemically amplified resists. The deprotection path is characterized as spatially heterogeneous, forming a “fuzzy blob”. A fundamental factor of LER formation is therefore the packing of these “fuzzy blobs” within the resist, and their subsequent reaction with the developer. Efforts to describe this packing are briefly discussed.

## INTRODUCTION

Current levels of line edge roughness (LER) in chemically amplified photoresists will soon contribute nearly 10 % of the critical dimension budget according to the International Semiconductor Roadmap [1]. Control and reduction of line edge roughness (LER) in future resists requires a fundamental understanding of the roles of solubility switching and developer interactions. For chemically amplified resists (CARs), the first step of imaging generates acid through exposure of a photoacid generator (PAG). Subsequent diffusion and reaction of the acid with the polymer matrix alters the solubility of the surrounding matrix. The initial distribution of acid is therefore controlled by the aerial image (see fig. 1). In the limit of a sharp aerial image, a sharp concentration gradient in photogenerated acid exists at the pattern edge. Acid diffusion in this limit can result in roughening and loss of dimensional control [2]. Increased aerial image spread reduces the gradient in acid concentration, and the effects of acid diffusion and reaction on pattern dimensions and LER are reduced significantly [3]. In all cases, the primary route to deprotection is acid diffusion and reaction.

The formation of heterogeneity in deprotection at the pattern edge is suggested by both simulation and theoretical models of CARs. Schmid et al. describe the distribution of deprotection in terms of the actions of individual acid molecules [4]. The sidewall morphology of two systems, each equivalently deprotected, depends on the concentration of acid. The imaged region consists of deprotection volumes defined by the spatial limits of deprotection created by each acid. Formed by a diffusion and reaction process, these volumes feature an internal level of heterogeneity, further compounded by imperfect packing of the volumes. A spatial map of deprotection at a pattern edge is therefore a collection of these deprotection volumes. To illustrate this point, Schmid et al. use a molecular level simulation to create two sidewall surfaces of equivalent deprotection. The resultant surface morphology varies with initial acid concentration, suggesting that the level of deprotection alone is not sufficient to describe morphology. However, spatial homogeneity is a difficult parameter to control experimentally without varying other parameters such as developer concentration and initial acid concentration.

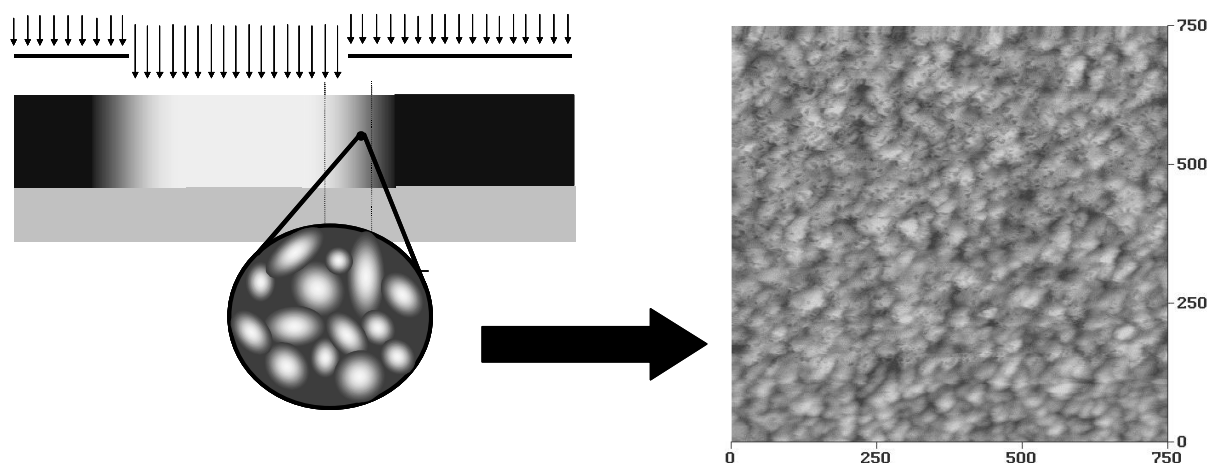


**FIGURE 1.** Schematic depicting the proposed relationship of the deprotection volume from individual acid diffusion and the resulting sidewall morphology. Shown on the left is the gradient in acid concentration, represented by the light (high acid) and dark (low acid) regions, created by the aerial image. Within the acid concentration gradient, acid diffusion and reaction creates a spatially inhomogeneous distribution of deprotection level. Immersion in a developer transforms this distribution into the observed sidewall morphology. Dimensions of AFM image are given in nanometers.

We provide results on the form of the deprotection volume created within a model photoresist polymer matrix using Small Angle Neutron Scattering (SANS). For this model resist polymer and PAG, the resulting volume is heterogeneous and characterized as following simple Brownian motion. The potential connection of these results to topological data from a model sidewall is also discussed.

## EXPERIMENTAL METHODS

Deprotection volume studies were conducted on films of partially deuterated poly(p-tert-butoxycarboxystyrene) (d-PBOCST) ( $M_{rn} = 21000$ , polydispersity = 2.1). Here, all hydrogens on the pendant tert-butoxycarboxyl group are isotopically substituted with deuterium, while hydrogens on the backbone and styrene ring remain. Synthesis of the d-PBOCST is described elsewhere [2]. The photoacid generator, di(t-butylphenyl) iodonium perfluorooctanesulfonate (PFOS) acid, was obtained from Day Chem [5]. Solutions of d-PBOCSt were prepared with varying loadings of added PFOS, where the total PFOS content was always  $< 1$  % mass fraction. Films were spin cast from solution in propylene glycol methyl ether acetate onto SEMI-standard 75 mm diameter wafers. The d-PBOCSt / PFOS films were blanket exposed to ultra-

violet radiation from a broadband source ranging between (220 and 260) nm with a total dose of  $500 \text{ mJ/cm}^2$ . Each film was subsequently baked on a hotplate at  $[90 \pm 1] \text{ }^\circ\text{C}$  for times ranging from [0 to 600] s [6]. The resulting level of deprotection was then determined as a function of PEB time with fourier transform infrared (FTIR) spectroscopy. A baseline concentration of photoacid generator (PAG) required initiate measurable deprotection was determined as  $\approx 0.5$  % mass fraction PFOS. This level is significantly higher than would normally occur in air controlled fabrication lines. Therefore, we consider only the mass fraction of PAG above the contamination level. Based on these measurements, processing conditions were chosen to provide a significant level of deprotection ( $[30 \pm 5]$  %) from a minimal concentration of PAG ( $[0.2 \pm 0.01]$  % mass fraction PFOS above the baseline concentration). A series of 22 nominally identical films were cast and processed with a post apply bake of  $[120 \pm 1] \text{ }^\circ\text{C}$  for  $[30 \pm 2]$  s, exposure energy of  $100 \text{ mJ/cm}^2$ , and PEB at  $[90 \pm 1] \text{ }^\circ\text{C}$  for  $[120 \pm 2]$  s. A second set of 22 films with zero added PFOS was processed under the same conditions.

Small Angle Neutron Scattering (SANS) measurements were performed at the NIST Center for Neutron Research on the NG-1 8 m SANS beamline. To reduce background scattering, all windows were

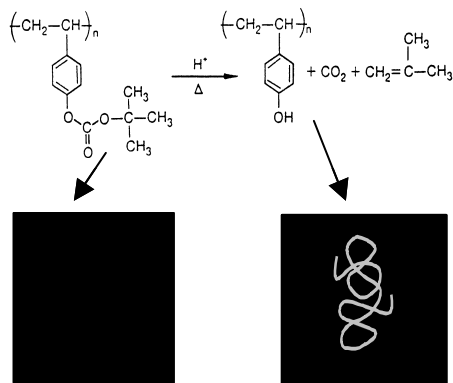


**Figure 2.** Schematic of the general deprotection reaction, showing the initial protected polymer PBOCST (left side of reaction) and its deprotected analog PHS (right side of reaction) and volatile by-products. In this study, the 9 hydrogens of the pendant sidechain are isotopically substituted with deuterium. The resulting change in neutron contrast is shown for a hypothetical deprotection path (bottom).

removed prior to measurement between the sample and detector, and the sample chamber was subsequently evacuated of air. Samples were measured at room temperature, with an average measurement time of 12 hours per sample. Initially, data is reduced by subtracting background measured from a stack of 22 clean silicon substrates, with corrections for detector sensitivity and dark current contributions. Intensity is placed on an absolute scale through comparisons of the direct beam flux through the samples as compared to that measured through vacuum, and further normalized by sample volume. The 2-dimensional data is then circularly averaged. In order to extract the scattered intensity due only to the path of deprotection, the intensity resulting from the “protected” samples (i.e. no added PFOS) is subtracted from that of the partially deprotected samples. The resulting form factor is schematically depicted in figure 3.

## RESULTS AND DISCUSSION

In figure 3, the scattered intensity from a partially deprotected d-PBOCSt sample is plotted as a function of scattering vector,  $q$ . The scaling of the data at high  $q$  follows a power law of the form  $I \sim q^{-D_{f,deprot}}$ , where  $D_{f,deprot}$  is the fractal dimension of the deprotection path. A fit to the data over the range  $q = [0.08 \text{ to } 0.11] \text{ \AA}^{-1}$  yields  $D_{f,deprot} = [2.2 \pm 0.4]$ . An ideal random walk possesses a fractal dimension of 2,

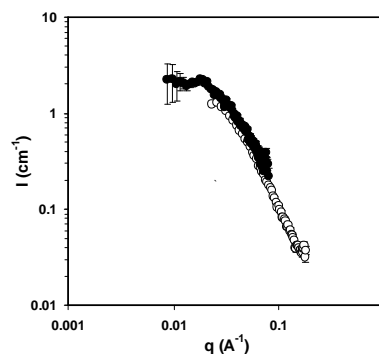


**Figure 3.** SANS Intensity as a function of scattering vector,  $q$ , for a partially deprotected d-PBOCST sample.

indicating that the radius of the random walk volume grows as  $N^{1/2}$ , where  $N$  is the number of steps in the walk. In contrast, a compact, space-filling walk would scale as  $N$ . As with the random walk, the deprotection path does not fill space efficiently. As a result, the interior volume of the deprotection volume is inhomogeneous with local areas of larger or smaller levels of deprotection. The volume is therefore characterized as a “fuzzy blob”.

Further information on the size and interactions of the deprotections paths are obtained from the correlation length,  $\xi$ . Here,  $\xi$  represents a distance of interaction of the deprotection path. In the limit of non-overlapping deprotection paths,  $\xi$  is approximately equal to the size of the deprotection volume. In figure 5, the data are presented as inverse intensity vs.  $q^2$  and fit to a line. The correlation length is obtained from the ratio of the slope and the intercept., where  $\xi = [12 \pm 1] \text{ nm}$ . The random walk scaling suggests the use of the Kratky limit as a more direct determination of deprotection volume size. In the limit  $qR_{G,deprot} \gg 1$ ,  $Iq^2$  is a constant. The data at lower  $q$  in figure 6 follow a typical Kratky form. Data in the region  $q > 0.06 \text{ \AA}^{-1}$  suffer from an overestimation of the background subtraction, making a precise determination of  $R_{G,deprot}$  difficult. Using the  $q$  value of maximum  $Iq^2$  indicated in figure 6, we estimate  $R_{G,deprot} (= [11.1 \pm 3] \text{ nm})$ . This value is consistent with the correlation length obtained from the Ornstein-Zernike analysis.

Characterization of chemically amplified resist sidewalls is often performed using topographic data from atomic force microscopy (AFM) measurements [7]. In the case of the d-PBOCST, the form of the resulting power spectrum follows a power law at high  $q$  with a characteristic length cutoff at  $d_{cutoff} \approx [25 \text{ nm}]$

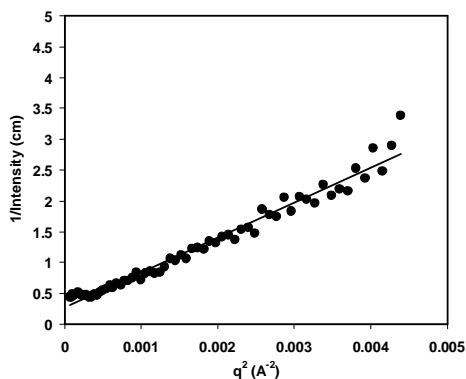


**Figure 4.** Inverse intensity as a function of  $q^2$ . Data are plotted in Ornstein-Zernike form, where a linear fit is used to extract the correlation length,  $\xi$  (solid line).

30] nm [8]. The cutoff is then consistent with the apparent “grain size” in the image of figure 1. The power law dependence of roughness at large length scales suggest the application of fractal mathematics to describe sidewall topology, where the slope on logarithmic axes is proportional to the fractal dimension of the surface,  $D_f$ . Observations of both increasing and decreasing fractal dimensions are reported for CARs in the limits of low dose, however  $D_f$  consistently plateaus at large doses.<sup>7,10</sup> Surface fractal dimensions scale from 2 (ideal flat plane) to 3 (space-filling). Increasing  $D_f$  represents increasingly heterogeneous surfaces. For CARs, the material origin of  $D_f$  is not currently understood. The transition between fractal and length-scale independent scaling indicates a cutoff of correlation in the formation of the surface morphology. The location of a correlation cutoff is often central to theories of surface formation. We propose that the origin of this cutoff is in part due to the packing of the deprotection volumes associated with individual acid molecules (see fig. 1). In this model, the form of deprotection establishes the length scale of heterogeneity of the surface.

If the cutoff is connected to the form of individual and non-interacting deprotection volumes, then their respective sizes are approximately equal. The data presented from SANS is used to predict the size and shape of the deprotection volume under a variety of processing conditions, including those used in the studies of model sidewalls. We use the measured deprotection volume size to calculate an effective diffusion-reaction coefficient of the acid. As an approximation, we assume the time to reach the PEB temperature is much smaller than the overall PEB time, allowing the use of the PEB time as the time of acid diffusion. The random walk form suggests a

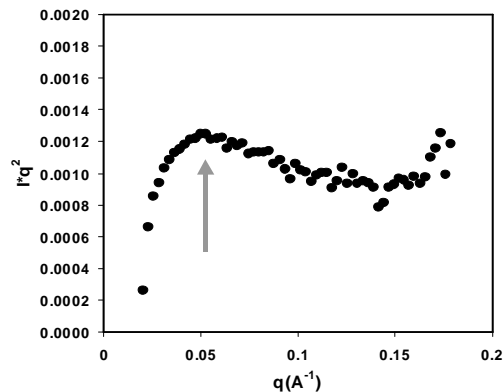


**Figure 5.** Kratky plot of SANS intensity ( $Iq^2$ ) as a function of  $q$  for a partially deprotected d-PBOCST sample. The crossover to the Kratky limit is estimate by the arrow.

simple Fickian representation where  $R_{G,deprot} = (2D_{deprot} t)^{0.5}$ , where  $t = 90$  s,  $R_{G,deprot} = 12$  nm, and  $D_{deprot}$  is a coefficient of diffusion-deprotection for the acid. The resulting value of  $D_{deprot}$  ( $\approx 1e-16$  cm<sup>2</sup>/s) is consistent with prior predictions based on experiments using the model bilayer [8]. For an order of magnitude approximation of  $R_{G,deprot}$  under different processing conditions,  $D_{deprot}$  is assumed independent of temperature. Applying  $D_{deprot}$  to the conditions used in the bilayer, where  $t = 90$  s, the predicted value of  $R_{G,deprot} = 5$  nm is consistent with estimations based on more extensive modeling in a different CAR. The size scale of the average deprotection volume associated with a single acid is therefore inconsistent with the cutoff length scale, where  $d_{cutoff} \approx [5 \text{ to } 6] R_{G,deprot}$ . The surface of a sidewall is therefore not describable as a collection of impenetrable deprotection volumes. The larger size of the cutoff length scale suggests that multiple deprotection volumes collectively interact with the developer to create the observed morphology. Further description will require further insight into collective phenomena and phase behavior due to developer-resist interactions.

## CONCLUSIONS

The form of the average deprotection volume created by individual acid molecules is determined using Small Angle Neutron Scattering (SANS). The form is consistent with a simple random walk and an effective diffusion-reaction coefficient on the order of  $1e-16$  cm<sup>2</sup>/s. Within this volume, the level of deprotection is spatially inhomogeneous. On average, a maximum in deprotection occurs at the center of the

volume, decaying to a background level at the edges. The volume is therefore described as a “fuzzy blob”. The interior of an imaged resist is then considered by a distribution function of fuzzy blobs, where the packing of the blobs determines the relative solubility in a developer solution. The final form of LER observed at model sidewall surfaces is not consistent with a simple model of individual, non-interacting and non-overlapping fuzzy blobs, indicating the need for further model refinement.

“Polymers for Micro- and Nano-electronics”, ACS Symp. 2003.

## ACKNOWLEDGMENTS

This work was funded in part by the DARPA Advanced Lithography Program under contract N66001-00-C-8803. Additional funding was provided by the NIST Office of Microelectronic Programs. R. L. J. and V. M. P. are supported by a NIST National Research Council postdoctoral fellowship.

## REFERENCES

1. “International Technology Roadmap for Semiconductors, 2001 Edition”, SIA 2001.
2. E. K. Lin, C. L. Soles, D. L. Goldfarb, B. C. Trinquet, S. D. Burns, R. L. Jones, J. L. Lenhart, M. Angelopoulos, C. G. Willson, S. K. Satija, W.-L. Wu, *Science* 297, 372-375, 2002.
3. W. D. Hinsberg, F. A. Houle, M. I. Sanchez, G. M. Walraff, *IBM J. Res. & Dev.* 45, 667-682, 2001.
4. G. M. Schmid, M. D. Smith, C. A. Mack, V. K. Singh, S. D. Burns, C. G. Willson, *Proc. of the SPIE* 4690, 381-390, 2002.
5. Certain commercial equipment and materials are identified in this paper in order to specify adequately the experimental procedure. In no case does such specification imply recommendation by the National Institutes of Standards and Technology nor does it imply that the material or equipment specified is necessarily the best available for this purpose.
6. The data in this manuscript, in the figures, and in the tables are presented along with the standard uncertainty ( $\pm$ ) involved in the measurement, where the uncertainty represents one standard deviation from the mean.
7. D. He and F. Cerrina, *J. Vac. Sci. Technol. B* 16, 3748-3751, 1998.
8. R. L. Jones, V. M. Prabhu, D. L. Goldfarb, E. K. Lin, C. L. Soles, J. L. Lenhart, W.-L. Wu, M. Angelopoulos, in